Mon. Not. R. astr. Soc. (1989) **237**, *Short Communication*, 55P–68P

Spectroscopic and photometric observations of SN1987A – V. Days 386–616

R. M. Catchpole,[1] P. A. Whitelock,[1] J. W. Menzies,[1] M. W. Feast,[1] F. Marang,[1] K. Sekiguchi,[1] F. van Wyk,[1] G. Roberts,[1] L. A. Balona,[1] J. M. Egan,[1] B. S. Carter,[1] C. D. Laney,[1] J. D. Laing,[1] J. H. Spencer Jones,[1] I. S. Glass,[1] H. Winkler,[2] A. P. Fairall,[2] T. H. H. Lloyd Evans,[1] M. S. Cropper,[3] M. Shenton,[4] P. W. Hill,[5] P. Payne,[2] K. N. Jones,[5] W. Wargau,[6] K. O. Mason,[3] C. S. Jeffery,[5] C. Hellier,[3] Q. A. Parker,[7] R. Chini,[8] P. A. James,[9] J. G. Doyle,[10] C. J. Butler[10] and G. Bromage[11]

[1] *South African Astronomical Observatory, PO Box 9, Observatory, 7935, South Africa*
[2] *Astronomy Department, University of Cape Town, Rondebosch 7700, South Africa*
[3] *Mullard Space Science Laboratory, Holmbury St Mary, Dorking, Surrey RH5 6NT*
[4] *Department of Physics, University of Keele, Staffordshire ST5 5BG*
[5] *University of St Andrews Observatory, Buchanan Gardens, St Andrews, Fife KY16 9LZ*
[6] *University of South Africa, PO Box 392, Pretoria 0001, South Africa*
[7] *Royal Observatory, Blackford Hill, Edinburgh EH9 3HJ*
[8] *Max-Planck Institute for Radio-astronomy, Auf dem Huegel 69, D-5300, Bonn 1, FRG*
[9] *Blackett Laboratory, Imperial College, Prince Consort Road, London SW7 2BZ*
[10] *Armagh Observatory, Armagh BT61 9DG*
[11] *Rutherford–Appleton Laboratory, Chilton, Didcot, Oxon OX11 0QX*

Accepted 1988 December 22. Received 1988 December 16

Summary. We present spectroscopic and $UBV(RI)_C JHKLM$ photometric observations of SN1987A in the Large Magellanic Cloud made at the Sutherland Observatory of the SAAO between days 386 and 616 after the Kamiokande–II neutrino event. During this period the bolometric flux from the supernova measured over the U to M wavelength range has continued to decline faster than the ^{56}Co decay rate. By day 560 the flux in this wavelength range accounts for only half of that expected from ^{56}Co decay. The estimated total flux (including X-ray and γ-ray data) is consistent with ^{56}Co remaining the sole energy source of the supernova over the period considered.

1 Introduction

Spectroscopic and photometric observations of SN1987A for the first 385 days after its discovery were presented by Menzies *et al.* (1987), Catchpole *et al.* (1987, 1988) and Whitelock *et al.* (1988) (hereafter Papers I, II, III and IV). In the present paper we give data for the period from day 386 to day 616 together with a brief discussion. As in papers II, III and IV we adopt the Kamiokande–II neutrino event as the epoch of the supernova outburst (JD 2446849.816, 1987 February 23.316). A distance modulus for the LMC of 18.5 and an interstellar absorption of $A_V = 0.6$ are also used.

2 Spectroscopic data

2.1 OBSERVATIONS 3500 Å TO 7500 Å

As previously, spectra have been obtained with a two-channel intensified Reticon detector on the grating Spectrograph at the Cassegrain focus of the 1.9-m telescope at Sutherland. A 300-line mm^{-1} grating was used in the first order with a slit width of 300 μm to give a resolution of 7 Å (FWHM). The instrumental flux calibration was obtained from an observation of a spectrophotometric standard each night. Once corrected to a flux scale, the supernova spectra were put on an absolute scale by multiplication by a suitable factor to give the same V magnitude as was observed on the 0.5-m telescope on the same night. The dates on which spectra were obtained are listed in Table 1. A selection of these at intervals of about 1 month are shown in Fig. 1, where a logarithmic flux scale has been used in order to represent both the emission lines and the relatively weak continuum adequately.

Table 1. Julian Date of spectroscopic observations of SN1987A (2440000 +).

March	7236.3	7239.3	7242.3	7250.3	
April	7257.2	7265.3	7269.4	7274.2	7279.3
May	7292.3	7295.2	7302.2	7310.2	
June	7317.2	7328.2	7340.6		
July	7350.6	7353.6	7354.6	7361.6	
August	7378.6	7376.7	7384.6	7393.6	7405.6
September	7422.5	7431.5			
October	7448.5	7453.5			

Throughout this whole interval, only minor changes have occurred in the appearance of the spectrum. With the decline in the continuum, the energy distribution has become progressively bluer. This is particularly noticeable in a comparison between the region around 6900 Å and that shortward of 3800 Å. A feature at about 7150 Å, which may be due to Ar I (see Filippenko 1988) has increased in strength relative to [Ca II] 7300 Å, throughout this period.

2.2 OBSERVATIONS 1.1–4.0 μm

The spectra shown in Fig. 2 were obtained on 1988 March 31, May 9 and August 16 (days 403, 442 and 541) with the SAAO filter-wheel spectrometer, at the Cassegrain focus of the 1.9-m telescope. They have a resolution ($\lambda/\delta\lambda$) of about 100 and were reduced as described in Paper III.

The hydrogen lines, most notably Brackett α and γ and Paschen β, faded much more rapidly than did other features during the period under discussion, continuing the trend noted in Paper IV. Similarly, the CO first overtone band at 2.3 μm had almost disappeared by day 541. The feature at 1.64 μm, due largely to [Si I] and [Fe II] with a minor contribution from Brackett 12, continued to strengthen relative to the other lines.

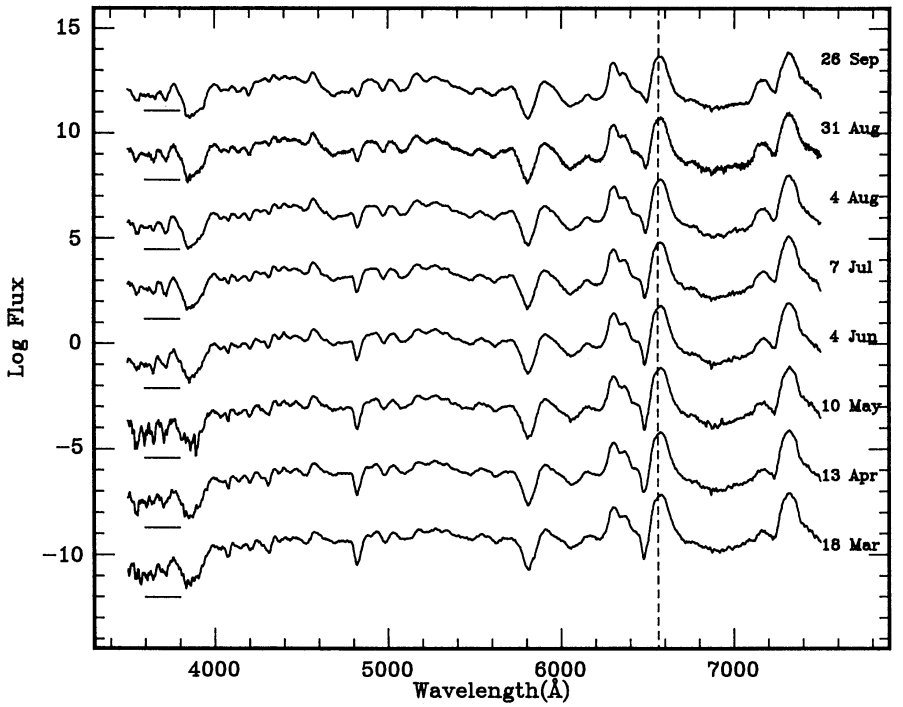

Figure 1. Spectra of SN1987A. Log flux (erg cm^{-2} s^{-1} $Å^{-1}$) is plotted against wavelength (Å). The short lines on the left side indicate the level of log $F_\lambda = -13$ for successive spectra. The vertical dashed line shows the laboratory wavelength of Hα.

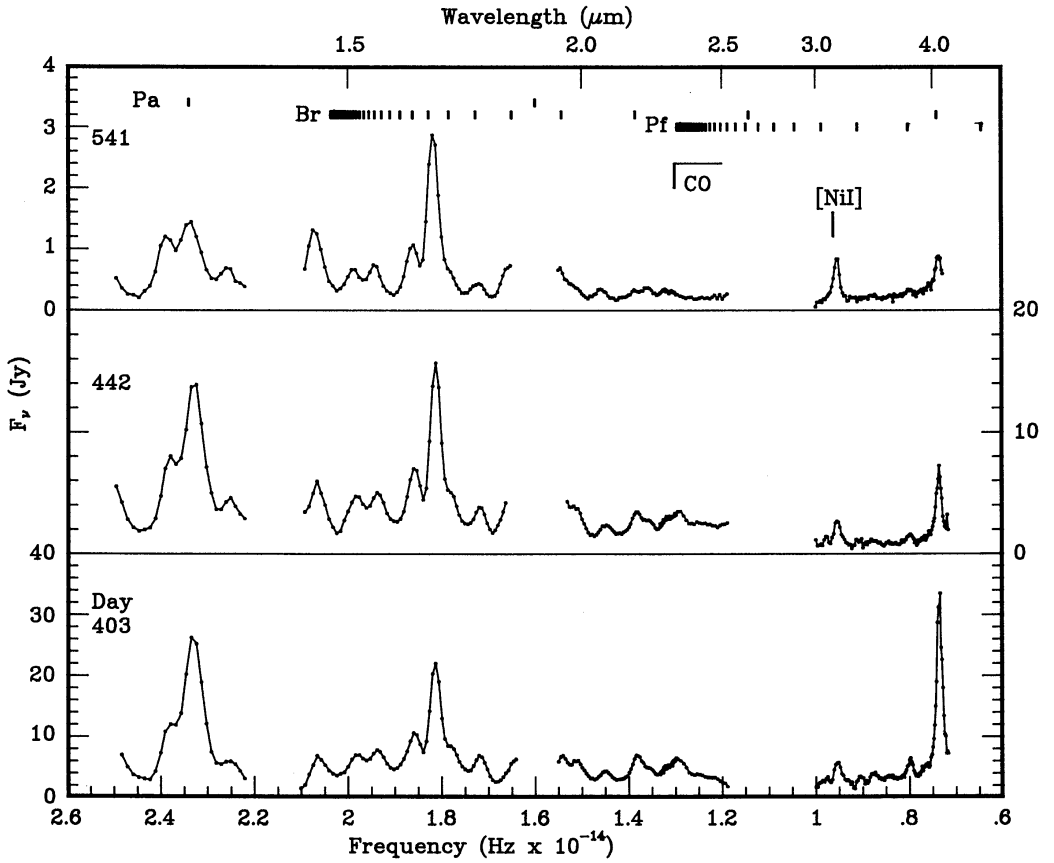

Figure 2. The infrared spectra obtained on days 403, 442 and 541. Note that the scales are different. In the top panel the three rows of short vertical ticks mark the positions of the lines in the Paschen, Brackett and Pfund series, respectively.

The continuum flux in the *L*-band relative to that in the *K*-band was more or less constant between May and August; however, the $(K-L)$ colour increased during this period due to the increasing equivalent width of the [Ni I] line at 3.12 μm (see Allen *et al.* 1988) which falls in the *L*-band.

Table 2. $UBV(RI)_C$ photometry of SN1987A.

JD 2447000+	V	(B-V)	(U-B)	(V-R)	(V-I)
236.247	6.861	1.027	1.032	1.050	1.470
237.253	6.870	1.022	1.044	1.038	1.460
239.253	6.892	1.023	1.031	1.044	1.462
240.253	6.906	1.012	1.032	1.052	1.466
241.255	6.906	1.018	1.029	1.039	1.450
242.255	6.924	1.006	1.028	1.046	1.458
243.251	6.926	1.011	1.028	1.040	1.446
244.251	6.937	1.000	1.025	1.029	1.433
246.246	6.961	1.003	1.009	1.030	1.431
247.243	6.970	0.999	1.008	1.028	1.430
248.241	6.985	0.992	1.011	1.029	1.427
250.244	7.002	0.991	0.975	1.014	1.420
251.242	7.010	0.992	0.996	1.020	1.410
252.237	7.018	0.994	0.974	1.014	1.415
253.244	7.030	0.992	0.971	1.032	1.408
259.258	7.081	0.980	0.950	0.994	1.393
260.234	7.103	0.975	0.938	1.002	1.399
261.364	7.114	0.968	0.949	1.000	1.392
262.230	7.119	0.970	0.934	0.996	1.394
263.232	7.138	0.958	0.936	0.998	1.396
264.234	7.139	0.965	0.936	0.994	1.377
265.264	7.149	0.957	0.943	0.998	1.371
266.282	7.163	0.958	0.935	1.001	1.381
267.232	7.177	0.954	0.931	0.987	1.374
268.229	7.187	0.953	0.921	0.982	1.375
270.226	7.209	0.947	0.918	0.980	1.359
274.232	7.249	0.938	0.886	0.976	1.358
275.234	7.263	0.945	0.882	0.972	1.357
278.239	7.29	0.93	0.87	0.96	1.34
279.333	7.31	0.91	0.86	0.98	1.36
280.375	7.31	0.93	0.88	0.96	1.33
281.245	7.325	0.917	0.872	0.964	1.323
282.235	7.339	0.927	0.851	0.962	1.334
283.232	7.343	0.922	0.872	0.960	1.324
284.229	7.355	0.907	0.876	0.960	1.317
286.218	7.381	0.900	0.856	0.956	1.328
287.212	7.389	0.917	0.855	0.949	1.312
288.213	7.393	0.909	0.849	0.949	1.317
289.212	7.411	0.901	0.865	0.948	1.301
290.211	7.42	0.90	0.85	0.93	1.30
291.221	7.434	0.902	0.852	0.940	1.301
292.226	7.449	0.897	0.838	0.941	1.283
297.222	7.491	0.895	0.800	0.931	1.275
298.217	7.52	0.88	0.81	0.95	1.29
299.242	7.525	0.889	0.807	0.927	1.283
311.259	7.681	0.885	0.755	0.924	1.266
317.256	7.744	0.845	0.768	0.903	1.244
321.670	7.80	0.87	0.87	0.88	1.24
322.670	7.81	0.85	0.75	0.88	1.23
323.200	7.80	0.85	0.77	0.88	1.22
328.216	7.866	0.826	0.712	0.872	1.208
329.222	7.872	0.834	0.700	0.865	1.202
330.224	7.880	0.842	0.687	0.853	1.190
331.219	7.896	0.832	0.688	0.856	1.182
334.238	7.94	0.82	0.70	0.86	1.20
334.672	7.98	0.81	0.69	0.84	1.18
336.673	7.964	0.806	0.695	0.861	1.188
337.638	7.97	0.83	0.70	0.85	1.15
343.660	8.057	0.798	0.650	0.814	1.144
353.656	8.146	0.780	0.63	0.778	1.124
354.650	8.212	0.780	0.655	0.780	1.111
355.657	8.224	0.769	0.611	0.785	1.117
356.634	8.233	0.766	0.616	0.792	1.109
357.660	8.248	0.763	0.585	0.797	1.121
359.626	8.277	0.762	0.600	0.793	1.110
362.652	8.316	0.753	0.584	0.772	1.092
364.628	8.345	0.752	0.581	0.763	1.097
365.632	8.364	0.754	0.573	0.779	1.094
366.632	8.379	0.743	0.566	0.773	1.087
367.632	8.394	0.748	0.562	0.776	1.082
368.620	8.413	0.732	0.576	0.787	1.083
369.644	8.42	0.73	0.58	0.78	1.06
370.643	8.45	0.73	0.57	0.79	1.05
372.628	8.464	0.729	0.536	0.764	1.070
373.646	8.482	0.730	0.526	0.757	1.072
374.650	8.501	0.722	0.516	0.764	1.051
376.622	8.537	0.720	0.527	0.753	1.068
377.630	8.556	0.708	0.519	0.762	1.052
378.636	8.570	0.708	0.508	0.754	1.048
379.619	8.584	0.718	0.502	0.754	1.050
380.634	8.598	0.710	0.498	0.751	1.049
382.636	8.64	0.69	0.50	0.74	1.05
383.632	8.648	0.700	0.486	0.732	1.040
384.630	8.666	0.691	0.474	0.739	1.038
385.642	8.676	0.690	0.460	0.735	1.012
386.634	8.700	0.688	0.456	0.731	1.024
388.619	8.74	0.69	0.45	0.73	1.02
389.646	8.749	0.684	0.444	0.723	1.011
390.636	8.77	0.68	0.44	0.73	1.01
393.634	8.821	0.678	0.418	0.710	0.990
394.642	8.850	0.666	0.433	0.718	1.015
399.593	8.938	0.661	0.408	0.697	0.977
408.552	9.103	0.612	0.352	0.677	0.970
408.643	9.100	0.624	0.346	0.675	0.970
409.596	9.116	0.620	0.333	0.671	0.958
410.578	9.148	0.626	0.359	0.672	0.967
411.615	9.174	0.611	0.340	0.675	0.967
412.524	9.19	0.61	0.36	0.68	0.96
416.491	9.273	0.595	0.330	0.674	0.968
417.516	9.295	0.592	0.326	0.672	0.972
422.491	9.390	0.574	0.290	0.652	0.941
425.499	9.449	0.551	0.252	0.641	0.930
426.537	9.472	0.549	0.240	0.643	0.922
427.583	9.483	0.528	0.226	0.630	0.908
428.612	9.508	0.540	0.220	0.634	0.918
429.526	9.515	0.545	0.199	0.628	0.913
431.562	9.572	0.525	0.200	0.623	0.929
435.540	9.670	0.502	0.208	0.622	0.923
436.508	9.690	0.509	0.173	0.619	0.920
437.530	9.708	0.502	0.180	0.615	0.910
438.446	9.721	0.500	0.193	0.616	0.898
439.561	9.74	0.49	0.16	0.61	0.90
444.534	9.85	0.48	0.13	0.59	0.89
448.413	9.945	0.468	0.140	0.602	0.898
452.479	9.998	0.444	0.086	0.588	0.897
453.580	10.027	0.446	0.080	0.576	0.888
455.459	10.082	0.450	0.115	0.582	0.886
458.460	10.135	0.455	0.081	0.571	0.888
460.410	10.164	0.412	0.104	0.567	0.896
461.522	10.184	0.427	0.056	0.566	0.882
462.428	10.211	0.418	0.055	0.580	0.912
464.398	10.247	0.402	0.058	0.578	0.903
466.422	10.275	0.414	0.069	0.552	0.887

3 Photometry

3.1 OBSERVATIONS

3.1.1 $UBV(RI)_C$ data

The $UBV(RI)_C$ data are listed in Table 2. As in Papers I, II, III and IV, these were all obtained with the single-channel photometer, standard filters and Hamamatsu R943-02 GaAs photomultiplier mounted on the 0.5-m reflector at Sutherland. Until JD 2447320, a 1.1-mag mask was used to reduce the supernova brightness; after that date a mask was unnecessary. As for previous papers, the data were reduced using standard colour equations. The zero point was determined from observations of two nearby standards CPD −68°375 and CPD −61°517. The magnitudes and colours of CPD −68°375 have been redetermined (Menzies & Laing 1987; Cousins 1987) and the following corrections should be added to all data given in Papers I–IV: $\delta V = -0.001$, $\delta(B-V) = -0.003$, $\delta(U-B) = +0.012$, $\delta(V-R) = +0.002$ and $\delta(V-I) = +0.001$. These changes have a negligible effect on the bolometric magnitudes published in those papers.

The standard errors of the magnitudes and colours in Table 2 should be less than 0.01 mag, except for data given to only two significant figures, in which cases problems were experienced with weather conditions.

It has been shown (Menzies 1988) that the discrepancy of up to 0.35 mag in I_C between mesurements made at CTIO and SAAO, which was noted by Hamuy *et al.* (1988a), results from the different effective pass-bands used at the two observatories. The CTIO *I* band is narrower than the SAAO one and gives very much lower weight to the very strong Ca II emission lines at ≃8600 Å and to the [Ca II] lines at ≃7300 Å.

Light curves for individual wavebands are shown in Fig. 3. The rate of decline in brightness increased progressively in all optical wavebands throughout the period considered here. The rate of decline was slowest in *U* and *B*, so the colours became bluer with time, as mentioned in Section 2.1.

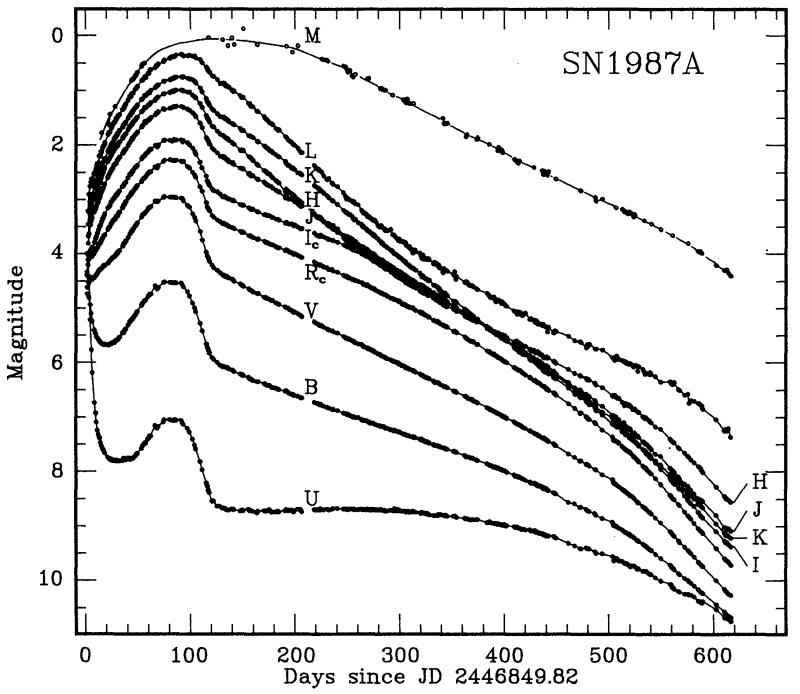

Figure 3. Light curves for SN1987A.

Table 3. *JHKL* photometry of SN1987A with 0.75 m.

JD 2447000+	J	H	K	L	JD 2447000+	J	H	K	L
236.25	5.397	5.385	5.376	4.808	342.21	6.761	6.426	6.908	
237.24	5.416	5.399	5.397	4.807	342.66	6.772	6.448	6.955	5.79
238.24	5.430	5.409	5.415	4.802	343.21	6.785	6.461	6.945	
239.23	5.438	5.425	5.426	4.804	343.65	6.803	6.459	6.961	5.79
240.24	5.458	5.434	5.446	4.800	347.21	6.851	6.500	6.994	
241.29	5.466	5.438	5.462	4.862	349.23	6.895		7.048	
242.24	5.485	5.458	5.474	4.895	353.21	6.933	6.559	7.100	
243.25	5.490	5.473	5.488	4.846	353.71	6.967	6.616	7.125	5.91
244.25	5.493	5.461	5.504	4.854	354.21	6.957	6.579	7.103	
245.52	5.50	5.45	5.54		354.68	6.976	6.602	7.132	5.91
246.25	5.522	5.485	5.531	4.878	355.21	6.92	6.57	7.09	
247.25	5.551	5.512	5.560	4.918	355.65	6.990	6.603	7.147	5.96
248.25	5.546	5.490	5.553	4.890	356.65	7.001	6.627	7.148	5.95
250.28	5.580	5.512	5.595	4.929	357.64	7.043	6.646	7.179	5.88
251.22	5.587	5.526	5.604	4.956	359.64	7.053	6.665	7.185	5.94
252.22	5.604	5.539	5.615	4.962	361.20	7.06	6.67	7.21	
253.25	5.623	5.550	5.633		362.62	7.119	6.727	7.271	
257.22			5.701		364.62	7.10	6.79	7.28	
259.21	5.689	5.618	5.726	5.047	365.63	7.167	6.753	7.319	
260.22	5.696	5.625	5.737	5.061	366.62	7.183	6.760	7.329	
261.50	5.69	5.60	5.71	5.06	367.64	7.196	6.770	7.334	
262.22	5.717	5.651	5.759	5.108	368.63	7.206	6.786	7.337	
263.22	5.736	5.661	5.779	5.073	369.64	7.206	6.777	7.370	
264.28	5.75	5.64	5.79		370.64	7.221	6.800	7.392	
265.23	5.76	5.66	5.80	5.11	372.64	7.290	6.857	7.416	
266.22	5.765	5.673	5.794	5.09	373.63	7.301	6.860	7.438	6.07
267.22	5.783	5.692	5.835	5.14	376.62	7.350	6.894	7.494	6.05
268.22	5.796	5.698	5.846	5.12	377.62	7.338	6.898	7.507	6.16
270.22	5.815	5.695	5.856	5.09	378.62	7.370	6.914	7.514	6.07
274.22	5.874	5.756	5.944	5.21	382.57	7.448	6.985	7.592	6.12
275.23	5.888	5.776	5.957	5.19	383.65	7.460	7.000	7.607	6.14
277.41	5.899	5.775	5.963		384.57	7.482	7.019	7.623	6.21
278.28	5.924	5.784	5.984	5.21	385.56	7.495	7.014	7.633	6.20
279.26	5.945	5.806	5.992	5.26	386.55	7.497	7.035	7.668	6.20
280.21	5.957	5.821	5.999	5.23	388.59	7.547	7.060	7.687	6.22
281.21	5.946	5.805	6.026	5.25	389.54	7.565	7.087	7.700	6.18
282.20	5.977	5.825	6.051	5.30	390.57	7.591	7.099	7.735	6.27
283.21	5.992	5.828	6.065	5.29	393.56	7.636	7.145	7.786	
284.21	5.995	5.851	6.082	5.30	394.57	7.683	7.179	7.803	6.26
286.24	6.021	5.867	6.107	5.36	398.55	7.70	7.20	7.86	
287.21	6.053	5.896	6.149	5.35	399.53	7.72	7.22	7.88	
288.21	6.058	5.916	6.166	5.31	408.55	7.937	7.403	8.056	6.35
289.21	6.066	5.907	6.167	5.37	409.66	7.963	7.432	8.067	6.39
290.22	6.06	5.90	6.18	5.36	410.33	7.993	7.454	8.080	6.43
291.21	6.086	5.916	6.191	5.46	411.48	7.995	7.456	8.105	6.40
292.19	6.09	5.92	6.21	5.35	412.51	8.010	7.471	8.145	6.36
296.20	6.125	5.943	6.244	5.50	413.55	7.94	7.45	8.10	
297.18	6.155	5.976	6.275	5.46	416.44	8.098	7.557	8.204	6.50
298.19	6.192	5.990	6.285	5.42	417.45	8.127	7.576	8.209	6.51
299.20	6.207	6.010	6.302	5.41	422.48	8.229	7.659	8.336	6.60
303.30	6.254	6.047	6.350		424.60	8.34	7.76	8.43	
307.20	6.344	6.118	6.452	5.53	425.57	8.299	7.703	8.352	6.58
311.20	6.367	6.127	6.471	5.52	426.48	8.316	7.740	8.418	6.75
313.64	6.357	6.132	6.500	5.62	427.49	8.319	7.749	8.445	
317.25	6.461	6.200	6.576	5.60	428.50	8.353	7.786	8.447	6.70
321.69	6.490	6.226	6.615	5.56	429.49	8.381	7.814	8.488	
322.21	6.504	6.243	6.638	5.61	431.49	8.408	7.840	8.504	6.71
323.21	6.520	6.250	6.645	5.63	435.58	8.499	7.914	8.604	6.74
327.62	6.566	6.290	6.694	5.71	438.40	8.516	7.980	8.637	6.82
328.22	6.582	6.286	6.709	5.73	439.58	8.544	8.010	8.660	6.85
329.20	6.602	6.313	6.730	5.67	440.56	8.58	7.98	8.67	
330.21	6.618	6.311	6.745	5.69	444.50	8.680	8.124	8.771	
331.19	6.619	6.322	6.769	5.66	448.41	8.71	8.17	8.89	
332.59	6.658	6.353	6.799		452.47	8.801	8.282	8.958	
334.22	6.666	6.363	6.815		455.47	8.874	8.332	9.019	
334.57	6.665	6.366	6.812	5.70	458.46	8.957	8.388	9.055	7.31
335.68	6.695	6.384	6.834		460.37	9.029	8.453	9.126	
336.22	6.700	6.380	6.833	5.72	461.38	9.028	8.470	9.172	
337.19	6.718	6.379	6.853	5.81	462.42	9.056	8.504	9.164	
339.23	6.751	6.429	6.895		464.37	9.038	8.521	9.195	
341.64	6.775	6.432	6.929	5.78	466.39	9.085	8.560	9.223	

3.1.2 JHKLL'M data

The *JHKL* photometry obtained with the 0.75-m telescope is listed in Table 3 and illustrated in Fig. 3. It has been reduced to the nearby standard HR1953 ($J=3.358$, $H=2.754$, $K=2.667$, $L=2.577$). Internal observational errors in J, H and K are 0.01 mag or less. As the supernova fades it has become increasingly difficult to measure L with high accuracy on the 0.75-m telescope and the errors have increased from about 0.03 to 0.06 over the interval. Whenever possible, observations have been made with the 1.9-m telescope and these are listed in Table 4. The 1.9-m observations are reduced to HR1953 ($J=3.328$, $H=2.754$, $K=2.667$, $L=2.577$, $L'=2.58$, $M=2.68$). The tabulated J magnitudes are on the 1.9-m natural system which accounts for the slightly different adopted J magnitude for HR1953. If the 1.9-m *JHK* magnitudes are used in place of the 0.75 m values then the calculated bolometric magnitudes are found to be 0.004 mag fainter on average.

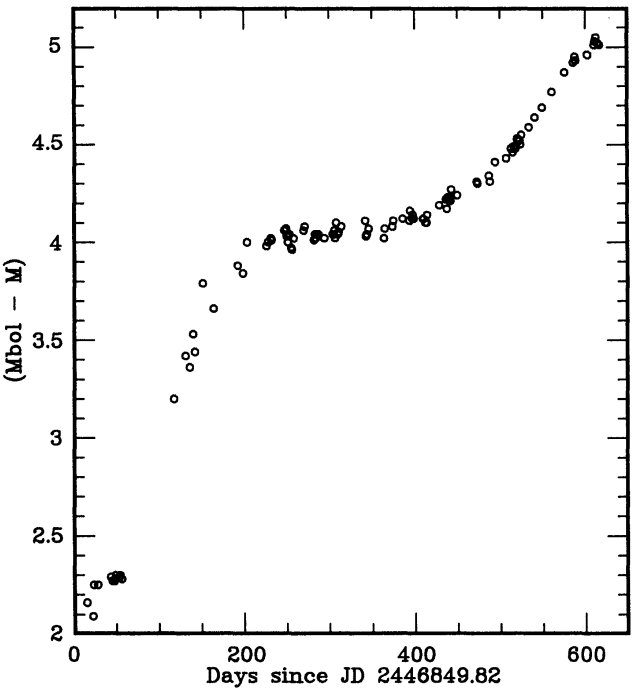

Figure 4. (M_{bol}–M) is shown as a function of time.

The proportional contribution of the M-band flux to the bolometric flux continues to increase and is illustrated by Fig. 4. At the same time, the rate of decline in M brightness has been very nearly constant between days 220 and 590, with a mean life of 111.83 ± 0.54 day, which happens to be very close to the mean life of ^{56}Co (111.26 day). This is illustrated in Fig. 5. The increase in the decline rate at M on about day 590 may be related to the decrease in decline rate in $UBVR_CI_C$ noted by Hamuy *et al.* (1988b).

Smith *et al.* (1988) note a factor of 2 increase in the 10–13 μm flux between days 464 and 517. Although this occurs at a time when M was brightening relative to M_{bol}, as shown in Fig. 4, there was no change in the behaviour of either (L–M) or (K–L). (L–M) has been almost constant at 2.8 since day 350, while (K–L) has increased steadily from 0.28 to 1.85 between days 275 and 616. This indicates that the 10–13 μm brightening did not extend to the near infrared.

1989MNRAS.237P..55C

Table 4. *JHKLL'M* photometry of SN1987A with 1.9 m.

JD 2447000+	J	H	K	L	L′	M	JD 2447000+	J	H	K	L	L′	M
243.31	5.530	5.454	5.488	4.862	4.12	2.10	343.69	6.828	6.473	6.972	5.770	5.20	2.99
244.29	5.528	5.461	5.501	4.862	4.11	2.04	356.21				5.890	5.30	3.14
246.26	5.578	5.508	5.557	4.904	4.13	2.12	362.59				5.958	5.43	3.18
247.23	5.559	5.495	5.552	4.904	4.14	2.10	364.56				5.992	5.44	3.23
248.24	5.573	5.506	5.568	4.907	4.15	2.14	365.60	7.161	6.735	7.300	5.987	5.43	3.23
251.25	5.605	5.517	5.603	4.940	4.17	2.12	366.62	7.171	6.755	7.312	6.010	5.45	3.24
252.21				4.947	4.17	2.14	367.63				6.014	5.43	3.26
253.23				4.976	4.20	2.17	368.67				6.021	5.46	3.26
264.28	5.762	5.644	5.798	5.074	4.30	2.29	369.68				6.031	5.46	3.23
278.30				5.218	4.52	2.41	370.64				6.020	5.47	3.25
286.24				5.324	4.63	2.47	372.66				6.060	5.50	3.28
287.25	6.056	5.864	6.111	5.301	4.64	2.54	373.70				6.077	5.52	3.32
288.24	6.071	5.890	6.139	5.331	4.64	2.48	374.70				6.062	5.51	3.28
289.24	6.089	5.895	6.166	5.335	4.64	2.51	383.56	7.407	6.997	7.590	6.163	5.64	3.39
290.24	6.099	5.894	6.176	5.350	4.65	2.51	390.53				6.216	5.68	3.45
291.30				5.436	4.68	2.55	398.50	7.691	7.190	7.834			
299.20	6.226	6.004	6.304	5.433	4.75	2.62	399.64	7.776	7.304	7.891	6.365	5.73	3.55
313.69				5.569	4.91	2.78	410.65				6.404	5.83	3.66
321.67	6.516	6.222	6.616	5.596	5.03	2.78	425.57	8.269	7.703	8.352	6.576	6.01	3.81
322.18	6.531	6.235	6.640	5.623	5.01	2.83	435.60	8.466	7.904	8.571	6.751	6.16	3.96
323.18	6.542	6.245	6.646	5.635	5.01	2.84	437.63	8.521	7.944	8.607	6.784	6.18	3.96
334.26	6.680	6.329	6.807	5.703	5.17	2.92	438.63				6.789	6.19	3.99
335.66	6.716	6.387	6.840	5.749	5.16	2.94	452.50				7.037	6.45	4.21
336.62				5.753	5.21	2.96	460.35	8.976	8.421	9.057	7.246	6.60	4.31
337.22	6.745	6.407	6.878	5.747	5.16	3.03	461.37	8.972	8.420	9.064	7.218	6.60	4.30
339.27				5.806	5.18	3.02	462.39	8.969	8.441	9.087	7.250	6.61	4.29
342.20	6.783	6.412	6.912	5.755	5.19	2.99	464.38	9.021	8.468	9.121	7.211	6.64	4.36

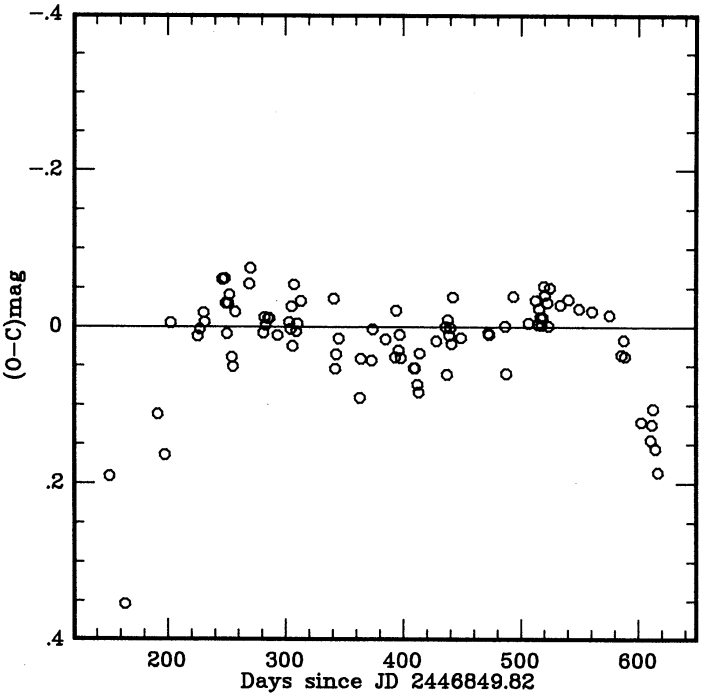

Figure 5. The residuals in the *M* magnitude from a straight line with the slope expected for the decay of ^{56}Co, are shown as a function of time. Note that there is no major change of slope at day 400, as seen in Fig. 4.

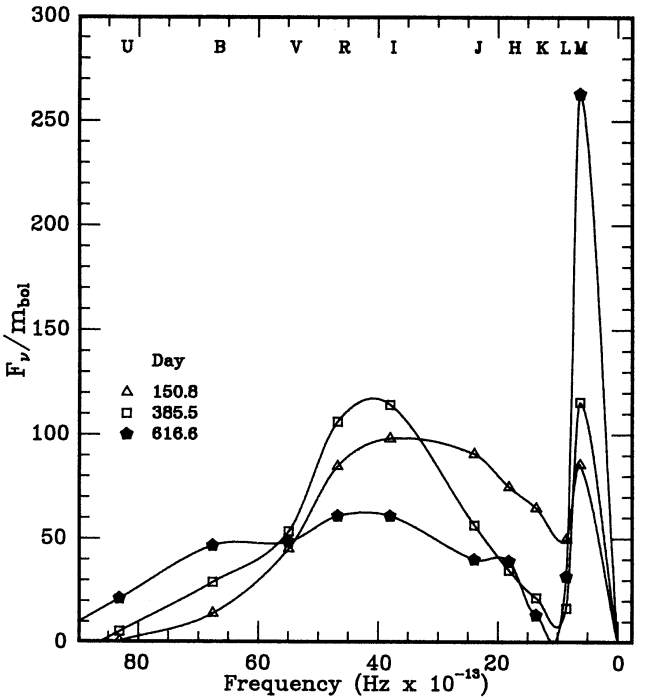

Figure 6. The changing shape of the flux distribution is shown for the three days indicated, during the steady decline phase of SN1987A.

3.2 BOLOMETRIC FLUX

The *U* to *M* flux distribution is shown in Fig. 6 for a number of days and illustrates the increasing contribution of the *M* band to the bolometric flux. Between *U* and *K*, the flux distribution is again assuming the shape of a blackbody distribution, as it did during the early

part of the supernova event (see Papers I and II), although the appearance of the spectra shows this to be due merely to the distribution of emission lines.

Table 5 gives four versions of the bolometric magnitude derived by integrating both spline and blackbody fits to the *U* to *L* and that to the *U* to *M* datasets. The methods of fitting to the data and the calibration of the fluxes in the various bands are discussed and referred to in Papers II, III and IV. We feel the most realistic representation of the bolometric magnitude is given by the spline fit to the *U* to *M* data. Note that by day 589 there is a difference of 0.2 mag between the spline fit to the *U* to *L* and the *U* to *M* data, which illustrates the importance of the

Table 5. Derived data for SN1987A.

Time	Bolometric Magnitude			
	U to L		U to M	
Day	bb	spline	bb	spline
386.43	6.05	6.23		
387.42	6.06	6.25		
389.41	6.08	6.27		
390.42	6.09	6.28		
391.47	6.10	6.29		
392.42	6.11	6.30		
393.43	6.12	6.31	6.12	6.20
394.43	6.14	6.32	6.13	6.20
396.43	6.16	6.35	6.16	6.23
397.43	6.17	6.36	6.17	6.24
398.43	6.19	6.37	6.18	6.26
400.44	6.21	6.40		
401.41	6.22	6.41		
402.41	6.23	6.42		
409.43	6.31	6.50	6.31	6.38
410.41	6.32	6.51	6.32	6.39
411.61	6.33	6.51		
412.40	6.34	6.53	6.34	6.41
413.40	6.36	6.55	6.36	6.43
414.44	6.37	6.55	6.36	6.43
415.43	6.38	6.57		
416.43	6.39	6.57		
417.41	6.41	6.59		
418.40	6.42	6.61		
420.40	6.44	6.63		
424.41	6.49	6.67		
425.41	6.50	6.69		
428.44	6.54	6.72	6.53	6.60
429.48	6.54	6.73		
430.47	6.56	6.75		
431.41	6.57	6.76		
432.40	6.59	6.78		
433.40	6.59	6.78		
434.40	6.61	6.79		
436.41	6.63	6.81	6.63	6.68
437.39	6.65	6.84	6.65	6.71
438.39	6.65	6.84	6.65	6.71
439.39	6.67	6.86	6.67	6.73
440.40	6.68	6.86	6.68	6.74
441.40	6.69	6.88	6.69	6.75
442.39	6.72	6.90	6.71	6.76
447.38	6.77	6.95		
448.38	6.78	6.96		
449.38	6.80	6.98	6.79	6.85
461.41	6.96	7.14		
467.43	7.03	7.21		
472.58	7.10	7.28	7.10	7.14
473.39	7.10	7.28	7.10	7.14
478.40	7.16	7.34		
479.39	7.18	7.35		
480.40	7.19	7.37		
481.39	7.21	7.38		
486.86	7.27	7.44	7.27	7.30
487.83	7.30	7.47	7.29	7.34

Time	Bolometric Magnitude			
	U to L		U to M	
Day	bb	spline	bb	spline
493.83	7.38	7.55	7.38	7.40
503.83	7.49	7.66		
504.83	7.55	7.72		
505.83	7.56	7.73		
506.82	7.57	7.73	7.57	7.58
507.83	7.58	7.75		
509.81	7.61	7.78		
512.83	7.66	7.83	7.66	7.66
514.81	7.69	7.85	7.69	7.69
515.81	7.71	7.87	7.71	7.71
516.82	7.72	7.89	7.73	7.72
517.81	7.74	7.90	7.74	7.74
518.80	7.75	7.92	7.76	7.75
519.82	7.77	7.93	7.77	7.76
520.82	7.79	7.95	7.80	7.78
522.80	7.81	7.97	7.82	7.80
523.82	7.83	7.99	7.83	7.82
524.82	7.85	8.01	7.86	7.83
526.80	7.89	8.04		
527.80	7.90	8.06		
528.81	7.92	8.08		
532.79	7.99	8.14		
533.81	8.01	8.16	8.01	7.98
534.78	8.02	8.18		
535.78	8.04	8.19		
536.77	8.06	8.21		
538.79	8.10	8.25		
539.78	8.11	8.26		
540.72	8.13	8.28	8.14	8.09
544.78	8.21	8.35		
549.74	8.31	8.44	8.32	8.24
558.78	8.47	8.60		
559.81	8.49	8.62		
560.75	8.52	8.65	8.53	8.43
561.72	8.54	8.66		
562.69	8.55	8.68		
566.65	8.63	8.76		
567.68	8.65	8.78		
572.66	8.75	8.88		
575.68	8.81	8.93	8.84	8.68
576.68	8.83	8.96		
578.68	8.87	8.99		
581.72	8.93	9.04		
585.75	9.02	9.13	9.05	8.88
587.76	9.06	9.17	9.10	8.91
588.70	9.08	9.18	9.11	8.92
589.75	9.09	9.20		
602.65	9.32	9.44	9.38	9.17
610.55	9.50	9.61	9.55	9.32
611.56	9.50	9.62	9.57	9.33
612.60	9.52	9.64	9.59	9.34
614.56	9.56	9.66	9.62	9.38
616.57	9.59	9.71	9.66	9.42

M band. The luminosity may be calculated from the tabulated bolometric magnitudes using the expression

$$L = 840 \times 10^{(40.0 - 0.4 \times m_{bol})} \text{ erg s}^{-1},$$

which assumes the distance modulus of SN1987A is 18.5 (note an incorrect value of 838 instead of 840, was used in Paper IV).

The problem of using broad-band photometry to estimate the bolometric flux of SN1987A at times when its spectrum is dominated by emission lines was discussed in Paper IV. The problem remains, especially now that so much flux is coming out in the *M* band. It may eventually be possible to use spectrum scans to help improve bolometric luminosity estimates.

The accuracy of the spline fitting in the region of the *M* band can be judged by integrating the 2–12 μm mid-April (day 412) spectrum given by Witteborn *et al.* (in preparation) and comparing it with the integral of our spline fit to the broad-band photometry for the same day. Our spline integral is brighter by 0.04 in the bolometric magnitude for that day. This is very good agreement, considering that the observational techniques and calibrations are so different. A spectrum in the 8–13 μm region obtained by Roche *et al.* (1988) on day 578 has a flux that exceeds the extrapolation of our *U* to *M* spline fit by an amount that, if included in the bolometric flux, would increase the brightness by 0.2 mag. If the excess flux observed in this band arises from a light echo, as suggested by Roche *et al.*, it should not be included in the total bolometric flux and we have accordingly ignored it. It is worth noting that the wavelength transmission function for the *M* band given by Glass (1973) lies to the red of the band head of CO, which may result in our slightly underestimating the contribution of the CO emission to the bolometric flux.

4 Discussion

As the supernova continues to fade, the possibility of contamination of the photometry by nearby stars becomes increasingly likely. Hamuy *et al.* (1988b) suggest that contamination may be affecting their photometry. There is some evidence that a faint star may be interfering with our 0.75-m infrared photometry. This effect may be detectable in the *JHK* photometry as early as day 500 but only becomes significant after day 600, when it amounts to an underestimate of about 0.07 mag of brightness in the *K* band. This will cause the bolometric magnitude to be underestimated by 0.01 mag on day 616, which will have no effect on the findings of this paper.

In Paper III we showed that, in the interval from day 147 to day 260, the bolometric flux from SN1987A declined at a rate characteristic of the radioactive decay of ^{56}Co. Since about day 285, the bolometric flux deduced from the *U* to *M* data declined progressively faster than expected for the decay of ^{56}Co. The difference is shown in Fig. 7 as a dashed line; the straight line shows the expected flux from an assumed initial mass of 0.078 $M_\odot$ of ^{56}Co and the curved line the bolometric flux. There is some uncertainty in fitting the observed flux curve to the expected one and the hatched area shows the effect of a relative shift of ± 0.02 mag between the two.

X-rays as well as 837- and 1238-KeV line emission from SN1987A were observed unexpectedly early in 1987 mid-August. Most of the X-ray radiation comes from multiple Compton scattering of ^{56}Fe line emission, though there is a soft component below 10 KeV, of unknown origin. The *Ginga* satellite obtains measurements in the 2–30 KeV range relatively frequently, but only sporadic observations are made at higher energies by various detectors on the Kvant module of the Mir satellite, by the SMM satellite and by balloon- and rocket-borne detectors. Unfortunately, most of the high-energy radiation comes out at energies beyond 100

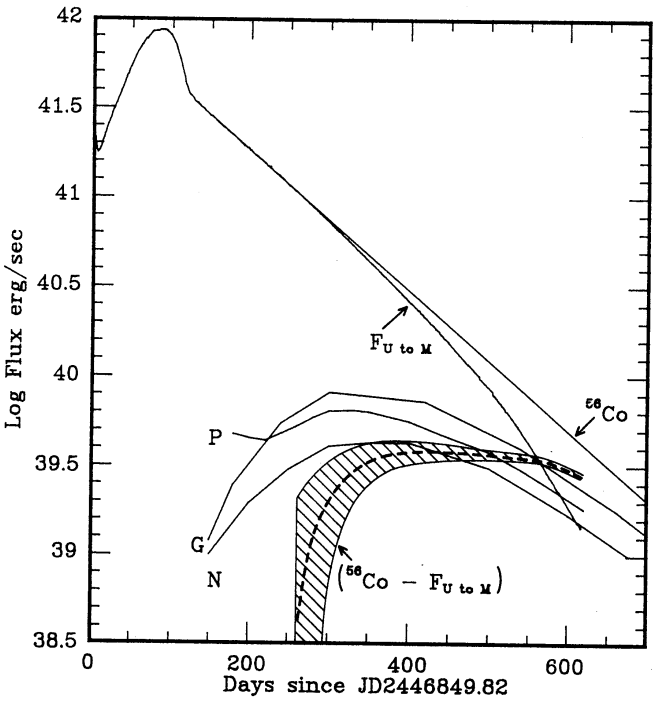

Figure 7. Comparison between flux expected from decay of 0.078 $M_\odot$ of ^{56}Co (straight line) and U to M bolometric flux curve for SN1987A (contiguous line). In constructing the observed flux curve, we have obtained M values where necessary from the smoothed K light curve and $(K-M)$ colour curve. The dashed line represents the difference (^{56}Co decay − bolometric flux) and the hatched area shows the effect of an uncertainty of ±0.02 mag in fitting the observed to the expected curve. The lower three continuous lines show the predictions of models for the X- and γ-ray flux, as described in the text (P = Pinto *et al.* 1988; G = Grebenev & Sunyaev 1988; N = Nomoto *et al.* 1988).

keV and it is necessary to model the emission in this region. The flux levels in X- and γ-rays are low and this leads to relatively large observational errors.

A number of investigations have been undertaken to predict the X- and γ-ray output from SN1987A. They all start with models constructed to reproduce the bolometric flux curve. The early emergence of high-energy radiation led to the realization that mixing in the supernova envelope is important. Grebenev & Sunyaev (1988) and Pinto, Woosley & Ensman (1988) use different degrees of mixing, together with Monte Carlo simulations of photon transport, to derive flux curves which are constrained to fit the X- and γ-ray data up to about day 300. Beyond that time, their results are predictions of how the flux will change. Nomoto *et al.* (1988) have given their models a clumpy structure together with mixing and have adjusted their parameters to fit the Ginga X-ray data up to day 485. Nomoto (private communication) finds that his prediction for day 550 fall below the observed flux and further adjustments to the model are necessary. The high-energy flux curves derived by the three groups have been included in Fig. 7.

It is not practical to derive the total flux from SN1987A by adding the bolometric flux to the observed X- and γ-ray flux because of the low accuracy and sparse coverage of the latter. Instead, we have added the bolometric flux to the predictions from the models referred to above. The results are shown in Fig. 8 with, for comparison, the difference between the expected ^{56}Co flux and the bolometric flux. If the total flux declined at the ^{56}Co decay rate it would be represented by the horizontal line. The deviation of all three curves from the horizontal are remarkably small, bearing in mind that the Grebenev & Sunyaev and Pinto *et al.*

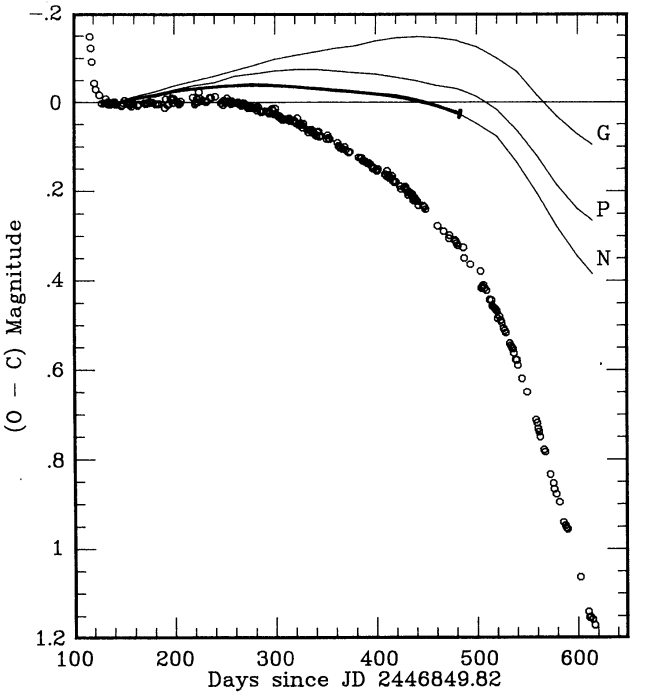

Figure 8. The individual points show the difference between the observed U to M bolometric flux (O) and the ^{56}Co decay curve (C). The bolometric flux uses M magnitudes determined as described in the caption to Fig. 7. (O − C) is given in magnitudes. The continuous curves show the result of adding our U to M bolometric flux curve to the X- and γ-ray fluxes predicted by three independent models indicated G, P and N as in Fig. 7. The Nomoto *et al.* model has been adjusted to fit the Ginga flux until day 485 and the curve until this date is represented by a heavy line. The horizontal line represents the ^{56}Co decay curve.

curves are predictions beyond day $\simeq 300$. The Nomoto curve begins to fall below the horizontal after day 485, but as noted above the observed X-ray flux is greater than predicted and the curve must be adjusted upward for day 550 and later.

Figs 7 and 8 emphasize different aspects of the comparison between the U to M bolometric flux and the models of the γ- and X-ray flux. The fact that the U to M flux is now below the predictions of all the models leaves open the possibility that a significant amount of flux is escaping in other wavelength regions.

On day 560 the total bolometric flux is divided amongst the various spectral regions as follows: γ- and X-ray 50 per cent, U to L 40 per cent and L through M 10 per cent. It is important to realize that individual γ- and X-ray observations are subject to observational errors of about 40 per cent or more and these uncertainties may provide the most serious constraint on our ability to detect a pulsar in the system based on the shape of the total bolometric flux curve.

There seems to be no evidence at this stage for an extra energy source, such as a pulsar, in SN1987A.

5 Acknowledgments

We thank Dave Kilkenny for some observations and for supervising the reduction of the optical photometry. We also thank the technical staff at Sutherland for their continued competent handling of the frequent instrument changes required on the 1.9-m telescope during this interval.

References

Allen, D., Spyromilio, J., Meikle, P. & Varani, G., 1988. *IAU Circ. No. 4623.*
Catchpole, R. M. *et al.,* 1987. *Mon. Not. R. astr. Soc.,* **229,** 15P (Paper II).
Catchpole, R. M. *et al.,* 1988. *Mon. Not. R. astr. Soc.,* **231,** 75P (Paper III).
Cousins, A. W. J., 1987. *S. Afr. astr. Obs. Circ.,* **11,** 89.
Filippenko, A. V., 1988. *Proc. Fourth George Mason Astrophysics Workshop,* p. 106, eds Kafatos, M. & Michalitsianos, A., Cambridge University Press, Cambridge.
Glass, I. S., 1973. *Mon. Not. R. astr. Soc.,* **164,** 155.
Grebenev, S. A. & Sunyaev, R. A., 1988. *Soviet Astr. Lett.,* **14,** 675.
Hamuy, M. I., Suntzeff, N. B., Gonzalez, R. & Martin, G., 1988a. *Astr. J.,* **95,** 63.
Hamuy, M. I., Suntzeff, N. B., Martin, G. & Gonzalez, R., 1988b. *IAU Circ. No. 4860.*
Menzies, J. W. *et al.,* 1987. *Mon. Not. R. astr. Soc.,* **227,** 39P (Paper I).
Menzies, J. W. & Laing, J. D., 1987. *Mon. Not. R. astr. Soc.,* **231,** 1047.
Menzies, J. W., 1989. *Mon. Not. R. astr. Soc.,* **237,** 21P.
Nomoto, K., Shigeyama, T., Kumagai, S., Itoh, M., Nishimura, J., Hashimoto, M., Saio, H. & Kato, M., 1988. *Physics of Neutron Stars and Black Holes,* ed. Tanaka, Y., Universal Academy Press, Tokyo.
Pinto, P. A., Woosley, S. E. & Ensman, L. M., 1988. *Astrophys. J.,* **331,** L101.
Roche, P. F., Aitken, D. K., Smith, C. H. & James, S. D., 1988. Preprint.
Smith, C., James, S., Aitken, D., Orton, G. & Roche, P., 1988. *IAU Circ. No. 4645.*
Whitelock, P. A. *et al.,* 1988. *Mon. Not. R. astr. Soc.,* **234,** 5P (Paper IV).